Two Heptacopper(II) Disk Complexes with a $[Cu_7(\mu_3\text{-}OH)_4(\mu\text{-}OR)_2]^{8+}$ Core

James J. Henkelis,[†] Leigh F. Jones,[†,‡] Marcelo P. de Miranda,[†] Colin A. Kilner[†] and Malcolm A. Halcrow*[,†]

†*School of Chemistry, University of Leeds, Woodhouse Lane, Leeds LS2 9JT, U.K..*
‡*School of Chemistry, NUI Galway, University Road, Galway, Ireland.*
Email: M.A.Halcrow@leeds.ac.uk

Reaction of CuX_2 ($X^- \neq F^-$) salts with 1 equiv of 3-pyridyl-5-*tert*butylpyrazole (HL) in basic methanol yields blue solids, from which disk complexes of type $[Cu_7(\mu_3\text{-}OH)_4(\mu\text{-}OR)_2(\mu\text{-}L)_6]^{2+}$ and/or the cubane $[Cu_4(\mu_3\text{-}OH)_4(HL)_4]^{4+}$ can be isolated by recrystallisation under the appropriate conditions. Two of the disk complexes have been prepared in crystalline form: $[Cu_7(\mu_3\text{-}OH)_4(\mu\text{-}OCH_2CF_3)_2(\mu\text{-}L)_6][BF_4]_2$ (**2**) and $[Cu_7(\mu_3\text{-}OH)_4(\mu\text{-}OCH_3)_2(\mu\text{-}L)_6]Cl_2{\cdot}xCH_2Cl_2$ (**3**$\cdot x$$CH_2Cl_2$). The molecular structures of both compounds as solvated crystals can be described as $[Cu{\subset}Cu_6(\mu\text{-}OH)_4(\mu\text{-}OR)_2(\mu\text{-}L)_6]^{2+}$ (R = CH_2CF_3 or CH_3) adducts. The $[Cu_6(\mu\text{-}OH)_4(\mu\text{-}OR)_2(\mu\text{-}L)_6]$ ring is constructed from six square pyramidal copper ions, linked by 1,2-pyrazolido bridges from the L^- ligands and by basal, apical-bridging hydroxy or alkoxy groups, while the central copper ion is bound to the four metallamacrocyclic hydroxy donors in a near-regular square planar geometry. The L^- ligands project above and below the metal ion core, forming two bowl-shaped cavities which are fully (R = CH_2CF_3) or partially (R = CH_3) occupied by the alkoxy 'R' substituents. Variable temperature magnetic susceptibility measurements on **2** demonstrated antiferromagnetic interactions between the copper ions, yielding a spin-frustrated S = ½ magnetic ground state that is fully populated below around 15 K. Electrospray mass spectrometry, UV/vis and EPR measurements imply that the heptacopper(II) disk motif is robust in organic solvents.

Supporting Information

Table S1 Selected bond distances in the crystal structures in this work.

Table S2 Hydrogen bond parameters in the crystal structure of **2**·2Et_2O.

Table S3 Selected bond angles in the crystal structures in this work.

Figure S1. Space-filling views of the $[Cu_7(\mu_3\text{-}OH)_4(\mu\text{-}OCH_2CF_3)_2(\mu\text{-}L)_6]^{2+}$ cation in **2**·2Et_2O, showing the occupancy of the bowl-shaped cavities by the 2,2,2-trifluoroethoxy substituents.

Figure S2 Electrospray mass spectra of **2** and **3**.

Table S4 Peak assignments in the mass spectra of **2** and **3**.

Chart S1 Diagram showing the six unique J values required to rigorously describe superexchange in **2**, and the simplified coupling schemes used to model the susceptibility data in the main paper.

Figure S3 UV/vis/NIR spectra of **2** in different solvents.

Table S5 The *d*-*d* peak parameters from the UV/vis spectra of **2**.

Figure S4 *X*-band EPR spectrum of **2** in CH_2Cl_2 at 115 K.

Table S1 Selected bond distances in the crystal structures in this work (Å). See Figs. 1 and 2 of the main paper for the atom numbering schemes employed. Symmetry code (i): 1–*x*, –*y*, 1–*z*.

2·2Et_2O		**3**·*x*CH_2Cl_2	
Cu(1)–O(5)	2.003(3)	Cu(1)–O(5)	2.020(4)
Cu(1)–O(6)	1.991(3)	Cu(1)–O(6)	1.997(4)
Cu(2)–O(5)	2.373(3)	Cu(2)–O(5)	2.402(4)
Cu(2)–O(7^i)	1.983(3)	Cu(2)–O(7^i)	1.935(4)
Cu(2)–N(13)	2.119(3)	Cu(2)–N(9)	2.119(4)
Cu(2)–N(20)	1.956(3)	Cu(2)–N(16)	1.931(4)
Cu(2)–N(36)	1.955(3)	Cu(2)–N(32)	1.960(4)
Cu(3)–O(5)	2.006(3)	Cu(3)–O(5)	1.973(4)
Cu(3)–O(6)	2.357(3)	Cu(3)–O(6)	2.307(4)
Cu(3)–N(28)	2.097(3)	Cu(3)–N(24)	2.098(4)
Cu(3)–N(35)	1.958(3)	Cu(3)–N(31)	1.947(4)
Cu(3)–N(51)	1.987(3)	Cu(3)–N(47)	1.965(4)
Cu(4)–O(6)	2.003(3)	Cu(4)–O(6)	1.996(4)
Cu(4)–O(7)	2.245(3)	Cu(4)–O(7)	2.176(4)
Cu(4)–N(21^i)	1.983(3)	Cu(4)–N(17^i)	1.955(5)
Cu(4)–N(43)	2.090(3)	Cu(4)–N(39)	2.087(4)
Cu(4)–N(50)	1.951(3)	Cu(4)–N(46)	1.932(4)
Cu(1)…Cu(2)	3.6498(5)	Cu(1)…Cu(2)	3.5875(6)
Cu(1)…Cu(3)	3.2056(5)	Cu(1)…Cu(3)	3.2131(6)
Cu(1)…Cu(4)	3.4317(5)	Cu(1)…Cu(4)	3.3517(6)
Cu(2)…Cu(3)	3.4466(7)	Cu(2)…Cu(3)	3.4373(9)
Cu(2)…Cu(4^i)	3.3818(7)	Cu(2)…Cu(4^i)	3.3323(8)
Cu(3)…Cu(4)	3.4783(7)	Cu(3)…Cu(4)	3.4038(8)

Table S2 Hydrogen bond parameters in the crystal structure of **2**·2Et_2O (Å, º). The hydroxyl H atoms were placed in calculated positions, so these parameters should be treated with caution. In particular the O–H bonds are artificially long. See Fig. 1 of the main paper for the atom numbering scheme employed. Symmetry code (i): 1–*x*, –*y*, 1–*z*.

	O–H	H...F	O…F	O–H…F
O(5)–H(5)…F(12)	1.00	2.33	3.058(4)	128.8
O(6)–H(6)…F(10^i)	1.00	2.37	3.040(4)	123.7

Table S3 Selected bond angles in the crystal structures in this work (º). See Figs. 1 and 2 of the main paper for the atom numbering schemes employed. Symmetry code (i): 1–*x*, –*y*, 1–*z*.

2·2Et_2O		**3**·*x*CH_2Cl_2	
O(5)–Cu(1)–O(6)	83.83(11)	O(5)–Cu(1)–O(6)	81.42(16)
O(5)–Cu(1)–O(6^i)	96.17(11)	O(5)–Cu(1)–O(6^i)	98.58(16)
O(5)–Cu(2)–O(7^i)	83.67(11)	O(5)–Cu(2)–O(7^i)	82.5(2)
O(5)–Cu(2)–N(13)	99.06(11)	O(5)–Cu(2)–N(9)	104.00(16)
O(5)–Cu(2)–N(20)	93.68(12)	O(5)–Cu(2)–N(16)	94.16(16)
O(5)–Cu(2)–N(36)	95.21(11)	O(5)–Cu(2)–N(32)	94.02(15)
O(7^i)–Cu(2)–N(13)	172.87(12)	O(7^i)–Cu(2)–N(9)	169.40(18)
O(7^i)–Cu(2)–N(20)	94.38(13)	O(7^i)–Cu(2)–N(16)	93.17(18)
O(7^i)–Cu(2)–N(36)	94.25(13)	O(7^i)–Cu(2)–N(32)	95.40(18)
N(13)–Cu(2)–N(20)	78.92(13)	N(9)–Cu(2)–N(16)	78.18(17)
N(13)–Cu(2)–N(36)	92.07(13)	N(9)–Cu(2)–N(32)	92.48(16)
N(20)–Cu(2)–N(36)	168.24(14)	N(16)–Cu(2)–N(32)	168.85(17)
O(5)–Cu(3)–O(6)	74.95(10)	O(5)–Cu(3)–O(6)	75.03(16)
O(5)–Cu(3)–N(28)	168.96(12)	O(5)–Cu(3)–N(24)	170.99(17)
O(5)–Cu(3)–N(35)	93.99(12)	O(5)–Cu(3)–N(31)	94.95(17)
O(5)–Cu(3)–N(51)	95.59(12)	O(5)–Cu(3)–N(47)	97.01(18)
O(6)–Cu(3)–N(28)	99.09(11)	O(6)–Cu(3)–N(24)	99.87(15)
O(6)–Cu(3)–N(35)	109.40(12)	O(6)–Cu(3)–N(31)	103.48(15)
O(6)–Cu(3)–N(51)	91.91(12)	O(6)–Cu(3)–N(47)	94.57(15)
N(28)–Cu(3)–N(35)	79.07(13)	N(24)–Cu(3)–N(31)	78.86(16)
N(28)–Cu(3)–N(51)	93.88(13)	N(24)–Cu(3)–N(47)	90.75(17)
N(35)–Cu(3)–N(51)	158.29(14)	N(31)–Cu(3)–N(47)	160.42(17)
O(6)–Cu(4)–O(7)	88.12(11)	O(6)–Cu(4)–O(7)	88.28(19)
O(6)–Cu(4)–N(21^i)	92.52(12)	O(6)–Cu(4)–N(17^i)	93.45(17)
O(6)–Cu(4)–N(43)	171.08(12)	O(6)–Cu(4)–N(39)	172.73(18)
O(6)–Cu(4)–N(50)	92.81(12)	O(6)–Cu(4)–N(46)	93.72(17)
O(7)–Cu(4)–N(21^i)	96.66(12)	O(7)–Cu(4)–N(17^i)	96.71(17)
O(7)–Cu(4)–N(43)	89.53(12)	O(7)–Cu(4)–N(39)	93.9(2)
O(7)–Cu(4)–N(50)	99.65(12)	O(7)–Cu(4)–N(46)	98.43(18)
N(21^i)–Cu(4)–N(43)	96.30(14)	N(17^i)–Cu(4)–N(39)	93.2(2)
N(21^i)–Cu(4)–N(50)	162.99(14)	N(17^i)–Cu(4)–N(46)	163.41(18)
N(43)–Cu(4)–N(50)	79.10(14)	N(39)–Cu(4)–N(46)	79.10(19)
Cu(1)–O(5)–Cu(2)	112.74(12)	Cu(1)–O(5)–Cu(2)	108.14(18)
Cu(1)–O(5)–Cu(3)	106.19(12)	Cu(1)–O(5)–Cu(3)	107.13(19)
Cu(2)–O(5)–Cu(3)	103.51(11)	Cu(2)–O(5)–Cu(3)	103.12(16)
Cu(1)–O(6)–Cu(3)	94.62(10)	Cu(1)–O(6)–Cu(3)	96.32(15)
Cu(1)–O(6)–Cu(4)	118.41(13)	Cu(1)–O(6)–Cu(4)	114.15(18)
Cu(3)–O(6)–Cu(4)	105.55(11)	Cu(3)–O(6)–Cu(4)	104.32(16)
Cu(2^i)–O(7)–Cu(4)	106.05(12)	Cu(2^i)–O(7)–Cu(4)	108.2(2)

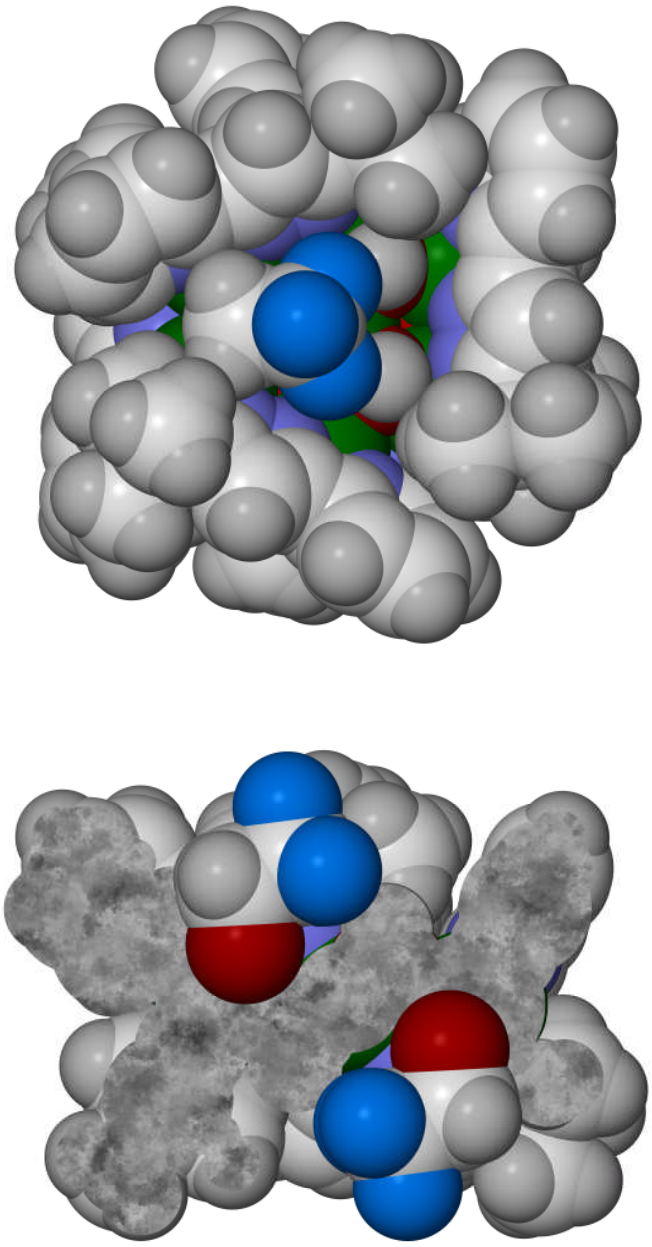

Figure S1 Space-filling views of the $[Cu_7(\mu_3\text{-}OH)_4(\mu\text{-}OCH_2CF_3)_2(\mu\text{-}L)_6]^{2+}$ cation in **2**·2Et_2O, showing the occupancy of the bowl-shaped cavities by the 2,2,2-trifluoroethoxy substituents. Top: view looking down into one cavity. Bottom: cutaway side view. The cutaway view is the same as in Fig. 3 of the main paper. Color code: C, white; H, pale gray; Cu, green; F, cyan; N, blue; O, red.

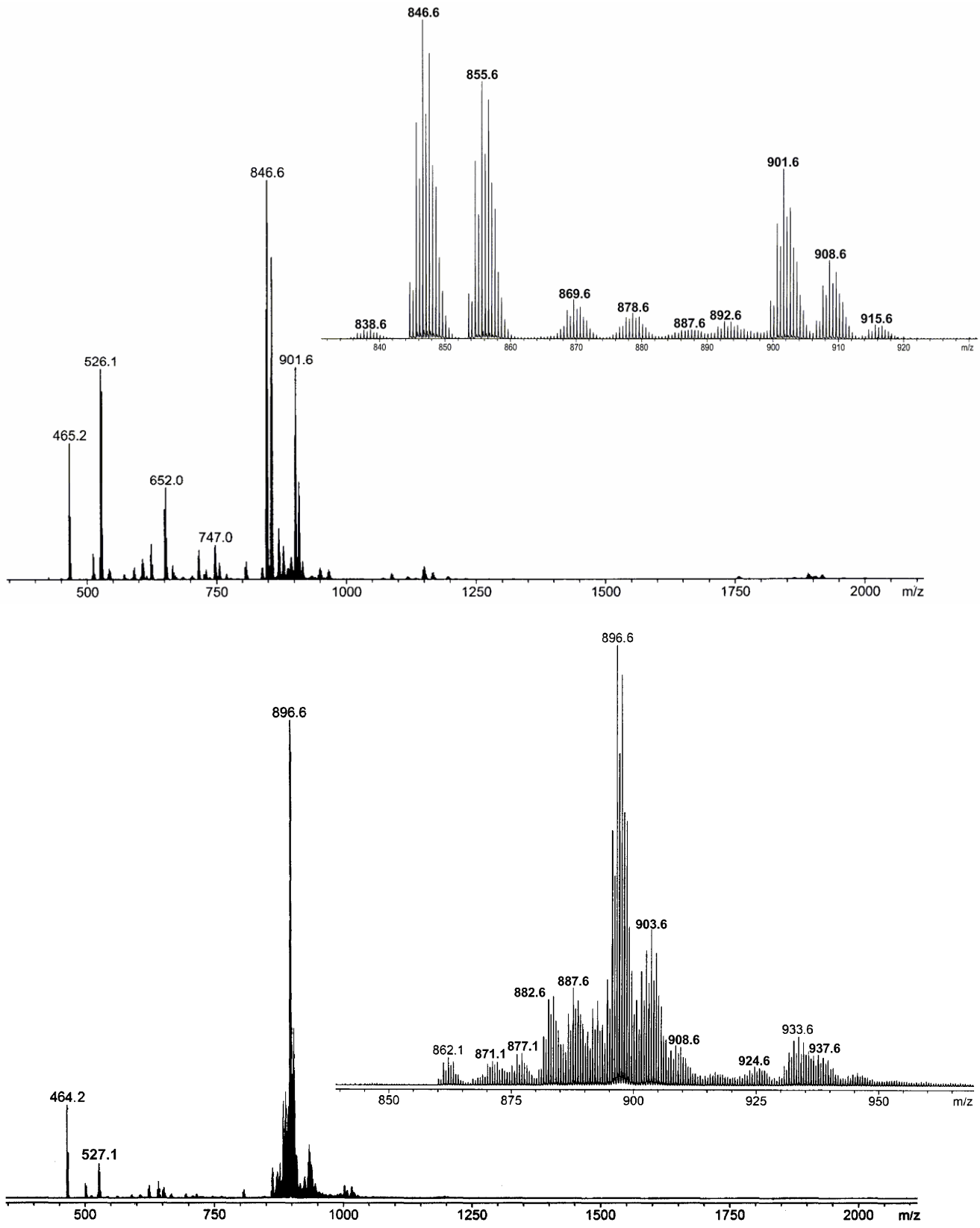

Figure S2 Electrospray mass spectra of **2** (top) and **3** (bottom). Peak assignments are listed in Table S4.

Table S4 Assignments of the mass peaks in the ES mass spectra of **2** and **3** (Fig. S2). The proposed molecular ions are consistent with the isotopic patterns in each peak, which are particularly diagnostic for the number of copper atoms present.

2		**3**	
m/*z*	Assignment	*m*/*z*	Assignment
465.2	$[Cu(LH)_2]^+$	464.2	$[CuL(LH)]^+$
526.1	$[Cu_2L_2]^+$	527.1	$[Cu_2L(LH)]^+$
652.0	$[Cu_3L_2O(O_2CH)]^+$	862.1	$[Cu_6(OH)_6L_6(MeCN)]^{2+}$
715.6	$[Cu_7(OH)_4(OCH_2CF_3)L_4(OH_2)]^{2+}$	871.1	$[Cu_6(OH)_6L_6(OH_2)(MeCN)]^{2+}$
747.0	$[Cu_7(OH)_3(OCH_2CF_3)_2L_4]^{2+}$	877.1	$[Cu_6(OH)_4(OMe)_2L_6(MeCN)]^{2+}$
756.0	$[Cu_7(OH)_3(OCH_2CF_3)_2L_4(OH_2)]^{2+}$),	882.6	$[Cu_7(OH)_6L_6(OH_2)]^{2+}$
838.6	$[Cu_6O(OH)_2(OCH_2CF_3)_2L_5(O_2CH)]^{2+}$	887.6[a]	$[Cu_7(OH)_4(OMe)_2L_6]^{2+}$
846.6	$[Cu_7O(OH)_2(OCH_2CF_3)_2L_5]^{2+}$	891.6	$[Cu_7(OH)_6L_6(OH_2)_2]^{2+}$
855.5	$[Cu_7(OH)_4(OCH_2CF_3)_2L_5]^{2+}$	896.6	$[Cu_7(OH)_4(OMe)_2L_6(OH_2)]^{2+}$
869.6	$[Cu_7O(OH)_2(OCH_2CF_3)_2L_5(O_2CH)]^{2+}$	903.6	$[Cu_7(OH)_4(OMe)_2L_6(MeOH)]^{2+}$
878.6	$[Cu_7(OH)_4(OCH_2CF_3)_2L_5(O_2CH)]^{2+}$	908.6[a]	$[Cu_7(OH)_4(OMe)_2L_6(MeCN)]^{2+}$
887.6[a]	$[Cu_7(OH)_4(OCH_2CF_3)_2L_5(O_2CH)(OH_2)]^{2+}$	916.6	$[Cu_7(OH)_4(OMe)_2L_6(OH_2)(MeCN)]^{2+}$
892.6	$[Cu_7O(OH)_2(OCH_2CF_3)_2L_5(O_2CH)_2]^{2+}$	924.6	$[Cu_7(OH)_4(OMe)_2L_6(MeOH)(MeCN)]^{2+}$
901.6	$[Cu_7(OH)_4(OCH_2CF_3)_2L_5(O_2CH)_2]^{2+}$	933.6	$[Cu_7Na(OH)_3(OMe)_2L_6(O_2CH)(MeCN)]^{2+}$
908.6[a]	$[Cu_7(OH)_4(OCH_2CF_3)_2L_5(O_2CH)(OH_2)(MeCN)]^{2+}$	937.6	$[Cu_7Na(OH)_4(OMe)_2L_6(O_2CH)(MeOH)]^{2+}$
915.5	$[Cu_7(OH)_5(OCH_2CF_3)L_6]^{2+}$		

[a]Although peaks with these masses appear in both spectra, we are confident that they arise from different species. Our differing assignments of these peaks for the two compounds agree with the other peaks in the each spectrum, which form two self-consistent series of adduct formation and fragmentation steps.

Chart S1 Left: the six unique *J* values required to rigorously describe superexchange in **2**. Right: the simplified coupling scheme used to model the susceptibility data in Fig. 4 of the main paper (eq 1; R = 2,2,2-trifluoroethyl and R' = *tert*butyl). The numbered copper ions correspond to those in the crystal structure of **2** (Fig. 1) and in eq 1.

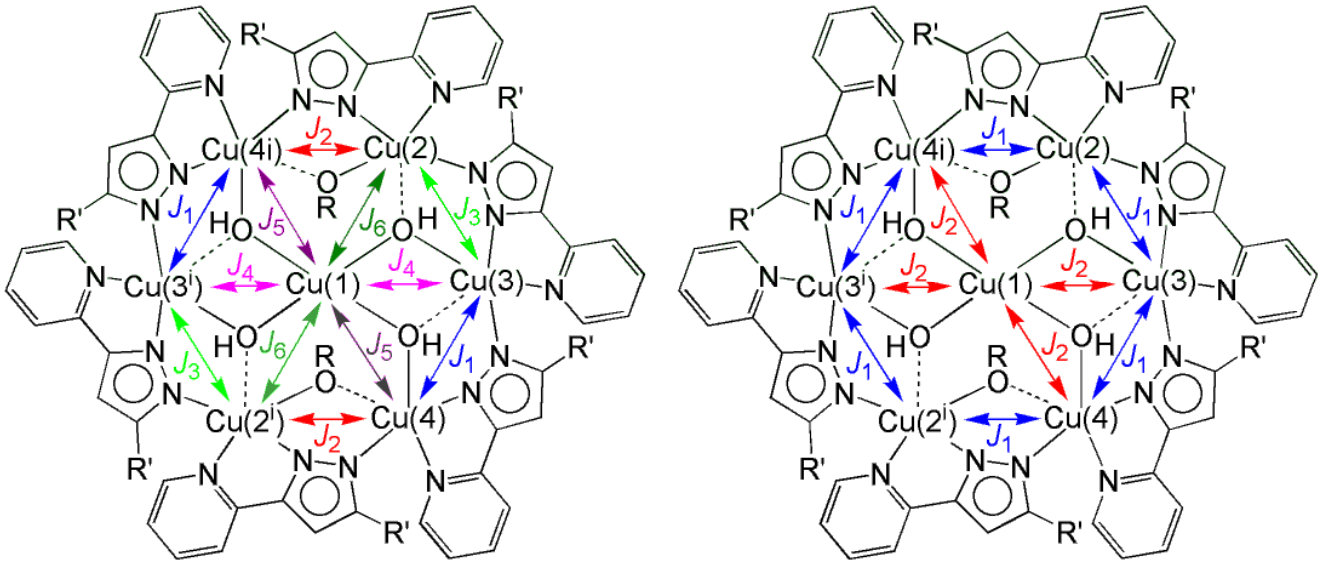

The Cu(1)...Cu(2)/Cu(1)...Cu(2^i) interaction was neglected in eq 1, because these copper ions are only linked by one basal, apical hydroxo bridging group.

The following, lower symmetry coupling scheme was also examined, to allow for the differences between the Cu(1)–O(5)–Cu(3) and Cu(1)–O(6)–Cu(4) bridging angles in the crystal structure of **2**·2Et$_2$O (Table S3).

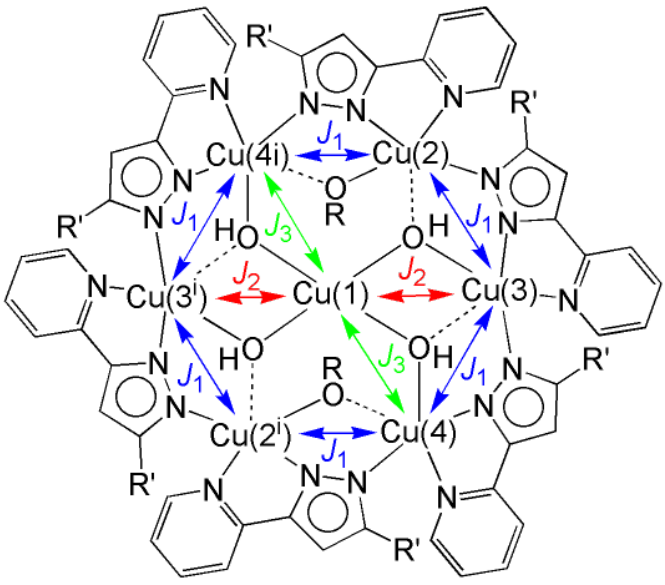

See the main text for further details.

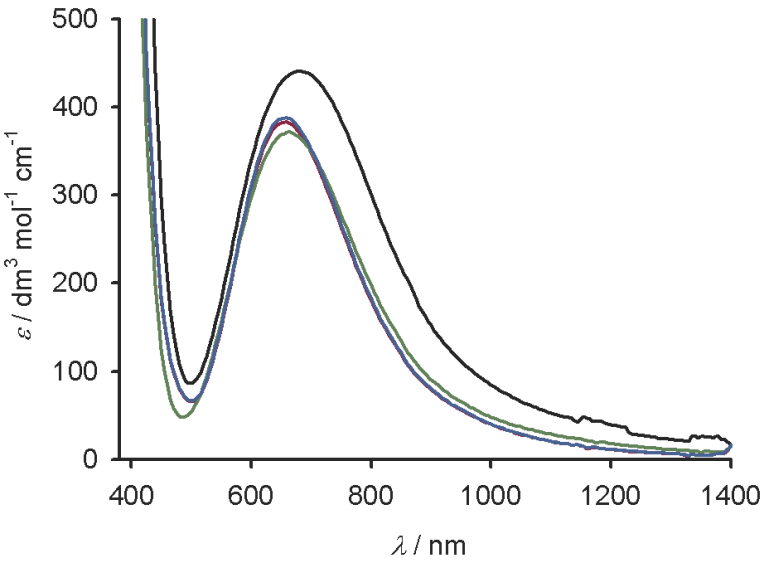

Figure S3 UV/vis/NIR spectra of **2** in MeOH (black curve), MeCN (green), $MeNO_2$ (red) and CH_2Cl_2 (blue).

Table S5 The *d-d* peak parameters from the UV/vis spectra of **2** (Fig. S3).

Solvent	λ_{max}, nm (ε_{max}, $dm^3\ mol^{-1}\ cm^{-1}$)
MeOH	680 (442)
MeCN	662 (372)
$MeNO_2$	657 (383)
CH_2Cl_2	657 (388)

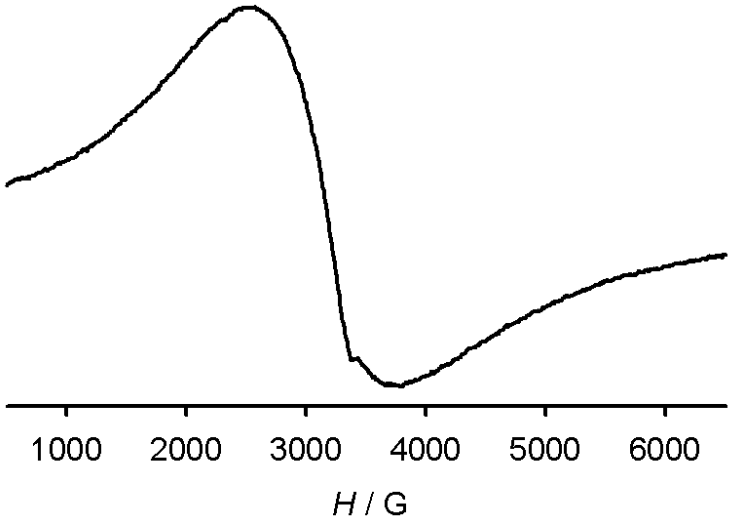

Figure S4 *X*-band EPR spectrum of **2** in CH_2Cl_2 at 115 K. The absence of any features around 3000 G, from the $g_{||}$ component of a mononuclear copper(II) impurity, is good evidence that the compound does not fragment significantly in this solvent (*c.f.* **1**; see ref. 4 from the main paper).